


The influence of Ni/Mg content of synthetic Mg/Ni talc on mechanical and thermal properties of waterborne polyurethane nanocomposites

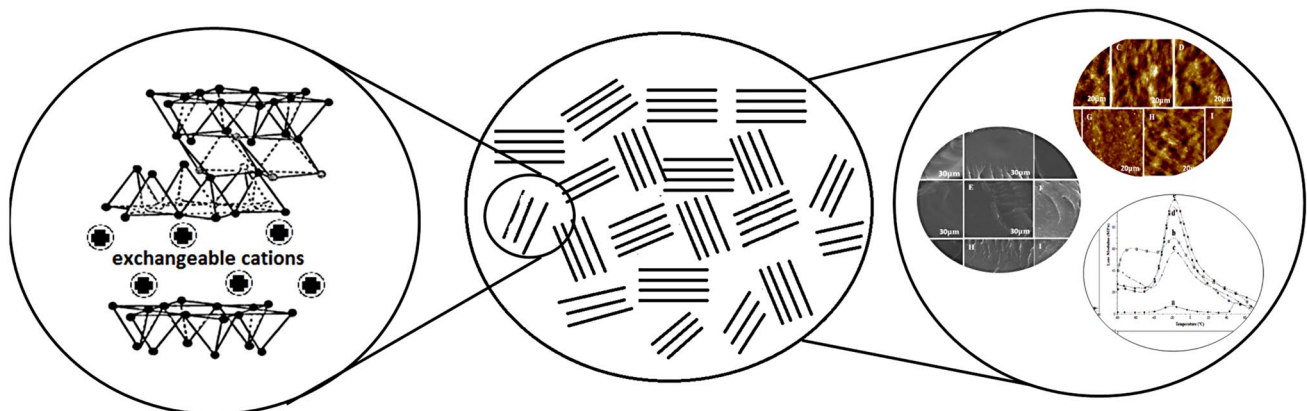
Manoela A. Prado¹ · Guilherme Dias¹ · Leonardo M. dos Santos² · Rosane Ligabue^{1,2} · Mathilde Poirier³ · Christophe Le Roux³ · Pierre Micoud³ · François Martin³ · Sandra Einloft^{1,2} 

Received: 3 December 2019 / Accepted: 29 April 2020 / Published online: 9 May 2020
© Springer Nature Switzerland AG 2020

Abstract

Waterborne polyurethanes (WPU) present interesting properties when compared to their solvent-based counterpart besides being organic solvent free. WPU also present some drawbacks such as low thermal and mechanical properties. The goal of this work was to synthesize and characterize new synthetic talc in a gel form with different magnesium (Mg) and nickel (Ni) ratios in their chemical structure $\text{Si}_4(\text{Mg}_x\text{Ni}_{1-x})_3\text{O}_{10}(\text{OH})_2$ with $0 < x < 1$ and to evaluate their influence on mechanical and thermal properties when used as filler in WPU matrix in order to obtain new nanocomposites as well. WPU/STMg_xNi_y nanocomposites were prepared by physical mixing and characterized by Fourier transform infrared spectroscopy (FTIR), X-ray diffraction (XRD), scanning electron microscopy (SEM), transmission electron microscopy (TEM), differential scanning calorimetry (DSC), thermogravimetric analysis (TGA), atomic force microscopy (AFM) and mechanical dynamic analysis (DMTA). Improvements in nanocomposites mechanical properties in relation to pristine WPU matrix were observed for samples with higher synthetic talc content. The variation of the amount of Mg and Ni in synthetic talc composition altered the storage and loss modules results being higher for nanocomposites obtained with synthetic talc samples with higher Ni content in their compositions. Tg varied according to synthetic talc content. Synthetic talc with different metal content in their composition changes WPU nanocomposites thermal and mechanical properties. These fillers can be used to design nanocomposites with desired applications.

Graphic abstract



✉ Sandra Einloft, einloft@pucrs.br | ¹Graduate Program in Engineering and Materials Technology (PGETEMA), Pontifical Catholic University of Rio Grande do Sul, Porto Alegre 90619-900, Brazil. ²School of Technology, Pontifical Catholic University of Rio Grande do Sul, Porto Alegre 90619-900, Brazil. ³ERT Geomaterials – GET UMR 5563 CNRS, University of Toulouse, 31400 Toulouse, France.



SN Applied Sciences (2020) 2:1047 | <https://doi.org/10.1007/s42452-020-2852-7>

Keywords Waterborne polyurethane · Synthetic STMg_xNi_y talc · Nanocomposites

1 Introduction

Polyurethanes (PU) are engineering materials finding different industrial application. In general PU are synthesized using organic solvents [1]. Due to environmental safety, organic solvents are gradually being replaced by water since the 1960s [1–5]. This solvent replacement initiative besides the manufacturing cost reduction helps to reduce volatile organic compounds (VOCs) emission into the environment [6]. WPU can find several application niches as adhesives, paint additives, coatings, sealants, medications, membranes, among others [7, 8]. WPUs present interesting properties when compared to their solvent-based counterpart, such as transparency, flexibility, abrasion resistance, non-flammability and high adhesion. The main disadvantage is related to low thermal and mechanical resistance [9–11]. Aiming to improve these properties the addition of nanofillers has been studied. Literature describes the incorporation of silica nanohybrids [12], TiO_2 [13], cellulose nanofillers [14], Fe_2O_3 [15], Ni–Zn [16, 17], SiO_2 [18], carbon nanofillers [19], clays and carbon nanotubes [20], $\text{Ni}_{0.3}\text{Zn}_{0.5}\text{Fe}_2\text{O}_4$ nanoparticles [21], synthetic talc [22], ferrite nanoparticles [23–25], ZnO [24], graphite [26], graphene oxides [27], nanoclay [28, 29] functionalized clays [30].

Talc is a layered magnesium phyllosilicate mineral of chemical formula $\text{Mg}_3\text{Si}_4\text{O}_{10}(\text{OH})_2$ being used as nanofiller for composite materials preparation [31, 32] in order to reduce production cost, enhance physical and chemical properties and provide new functionality to polymer matrix [33, 34]. Crystal-chemistry of talc structure can be modified by fully or partly replacing the Mg metal by other metals. Temperature, time and pressure can also be controlled during hydrothermal synthesis in order to obtain the desired structure [35, 36]. Unlike hydrophobic natural talc, synthetic talc can be obtained in a gel form due to their hydrophilic character facilitating their use in water-based polymer matrix nanocomposite synthesis [31, 32, 35, 37]. Due to this myriad of possible synthetic talc structures and properties, these new materials can be used as fillers for solvent-based polyurethane nanocomposites [38, 39] as well as for WPUs nanocomposites [40] preparation resulting in fluorescent nanocomposites [40], magnetic nanocomposites [23, 41] among others possibilities.

The main goal of this work was the synthesis and characterization of new synthetic talcs in a gel form substituting the magnesium by nickel in the percentages of 25%, 50%, 75% and 100% in their chemical structure $\text{Si}_4(\text{Mg}_x\text{Ni}_{1-x})_3\text{O}_{10}(\text{OH})_2$ with $0 < x < 1$. Yet, the effect of Ni content on the nanocomposite WPU/synthetic talc

formation, thermal and mechanical properties was evaluated.

2 Materials and methods

2.1 WPU synthesis

WPU was prepared by prepolymer method. The dispersion preparation occurred in two steps. The first was the prepolymer formation by the mixture of linear polyester polyol, isofurone diisocyanate (IPDI) ($\text{NCO}/\text{OH} = 1,7$) and dimethyl propionic acid (DMPA) solubilized in *n*-methylpyrrolidone. The mixture was kept in a closed system, at 85 °C, under mechanical stirring (500 rpm) for 1 h. Free NCO content was monitored by titration with *N*-dibutylamine (based on the ASTM 2572 standard). Once the desired free NCO content was reached, the temperature was reduced and maintained at 60 °C and triethylamine (TEA) was added. TEA addition was performed under mechanical stirring at 500 rpm for 15 min in order to neutralize the ionic groups generated by DMPA addition. The second reaction step was the neutralized prepolymer dispersion in a mixture of water/chain extender (hydrazine) under mechanical stirring (250–500 rpm) at 10 °C of temperature for 30 min. The dispersion solid content was 33%.

2.2 Synthetic talc synthesis

$\text{Si}_4(\text{Mg}_x\text{Ni}_{1-x})_3\text{O}_{10}(\text{OH})_2$ synthetic talc with $0 < x < 1$ was obtained by hydrothermal reaction as previously described [31, 42, 43]. The reactants ratio used in synthetic talc synthesis were based on the chemical formula of natural talc ($\text{Mg}_3\text{Si}_4\text{O}_{10}(\text{OH})_2$). When using different metals the reactants are mixed in stoichiometric proportions based on the chemical formula: $\text{Si}_4(\text{Mg}_x\text{Ni}_{1-x})_3\text{O}_{10}(\text{OH})_2$ with $0 < x < 1$, Si/Mg–Ni = 4/3 [44, 45]. In order to synthesize the talc–Ni, the substitutions of magnesium by nickel were performed from 25 to 100%, as shown in Table 1.

To synthesize the talc samples, the Si source was sodium metasilicate pentahydrate ($\text{NaSiO}_3 \cdot 5\text{H}_2\text{O}$), the Mg source was magnesium acetate tetrahydrate ($\text{Mg}(\text{CH}_3\text{COO})_2 \cdot 4\text{H}_2\text{O}$) and the Ni source was nickel acetate tetrahydrate ($\text{Ni}(\text{CH}_3\text{COO})_2 \cdot 4\text{H}_2\text{O}$). Sodium acetate (CH_3COONa) was used as catalyst for all reactions. Two solutions were prepared; first the Si source was solubilized in water and mixed to the catalyst. The Mg and/or Ni source (according to desired percentage) was solubilized in water and mixed with acetic acid (CH_3COOH). The two solutions were mixed under magnetic stirring and ultrasonicated

Table 1 Talc chemical formulas according to the substitution percentage of the Mg cation for Ni

Replacement ratio (%)	Talc chemical formula	Adopted nomenclature
0	$\text{Mg}_3\text{Si}_4\text{O}_{10}(\text{OH})_2$	–
25	$\text{Mg}_{2,25}\text{Ni}_{0,75}\text{Si}_4\text{O}_{10}(\text{OH})_2$	ST25Ni
50	$\text{Mg}_{1,5}\text{Ni}_{1,5}\text{Si}_4\text{O}_{10}(\text{OH})_2$	ST50Ni
75	$\text{Mg}_{0,75}\text{Ni}_{2,25}\text{Si}_4\text{O}_{10}(\text{OH})_2$	ST75Ni
100	$\text{Ni}_3\text{Si}_4\text{O}_{10}(\text{OH})_2$	ST100Ni

until a homogeneous mixture was obtained. The $\text{Si}_4(\text{Mg}_x\text{Ni}_{1-x})_3\text{O}_{10}(\text{OH})_2$ synthetic talcs were hydrothermally synthesized at 300 °C for 6 h under 86 bar of pressure. After the reaction, the obtained synthetic talc was withdrawn from the reactor in the gel form [35, 36].

2.3 WPU nanocomposites preparation

WPU nanocomposites were prepared by physical mixtures. A 100 g sample of WPU was placed under mechanical stirring (2000 rpm) for 30 min. The fillers ST25Ni, ST50Ni, ST75Ni e ST100Ni were added in different contents of 1% and 10% in relation to WPU weight. At the end, films of 70 μm of thickness were produced by molding.

2.4 Synthetic talc and nanocomposites characterization

WPU, synthetic talc and WPU nanocomposites films (thickness of 0.01 mm) were characterized by Fourier transform infrared spectroscopy/universal attenuated total reflectance (FTIR/UATR, PerkinElmer FTIR spectrometer model Spectrum100). The nanocomposites spectra acquisition data were performed in absorption mode in the range of 4000–400 cm^{-1} and for synthetic talc in the range of 10,000–400 cm^{-1} . WPU nanocomposites patterns for X-ray diffraction (XRD) were recorded on a Shimadzu XRD-7000 diffractometer equipment with CuK α Bragg–Brentano θ – θ geometry, between 5° and 80° with a step size of 0.02°, current of 40 kV and voltage of 30 mA. The talc standards were recorded in INEL CPS 120 powder diffractometer with CoK α 1 + 2 radiation between 0.334° and 127,206° 2 θ . Thermogravimetric (TGA) analysis of WPU and its nanocomposites were performed using a SDT equipment (TA Instruments model Q600). The tests were performed in a temperature ranging from 25 to 800 °C with a heating rate of 20 °C/min under constant N₂ flow. The TGA analyses were performed in triplicate. WPU samples and nanocomposites were analyzed by mechanical dynamic analysis (DMTA-TA Instruments Model Q800) for thermomechanical tests. Stress/strain tests were performed

at 25 °C. Loss modulus, storage modulus and tan δ were acquired utilizing a ramp from –80 to 80 °C. Mechanical tests were performed using rectangular films (0.15 mm thick, 12 mm long and 7.0 mm wide). The Young modulus of the materials was determined according to ASTM D638. Analyses were performed in triplicate. Scanning electron microscopy (SEM) images were emitted by scattered retroelectronic (BSE) mode on PHILIPS XL30 equipment, using gold for samples metallization. The films used for this characterization were of approximately 0.2 mm thick; transmission electron microscopy (TEM) was used to determine the particle size and morphology of nanocomposites. The samples were cryomicrotomed and analyzed on a Tecnai G2 T20 FEI operating at 200 kV. Atomic force microscopy (AFM) analyses were performed in peak touch mode using a PT Bruker Dimension Icon equipped with a TAP150A probe (Bruker, resonance frequency 150 kHz and spring constant of 5 N/m). The equipment was calibrated prior to sample measurements. The scanned area of the images was 5 \times 5 μm^2 with a resolution of 512 frames per area (LabCEMM/PUCRS).

3 Results and Discussion

3.1 FTIR Analysis

Infrared analyses for synthetic talc $\text{Si}_4(\text{Mg}_x\text{Ni}_{1-x})_3\text{O}_{10}(\text{OH})_2$ samples with different Ni contents are shown in Figs. 1 and 2.

Infrared spectrum for phyllosilicates undergoing partial replacement of Magnesium (Mg) by another divalent metal species shows a division in the hydroxyl stretch-up to four peaks, depending on the substitution degree [46–49]. The spectra presented in Fig. 1a and b show from high to low frequencies a random distribution of two metallic species (Mg and Ni), being the four bands related to the OH ion vibrating near the 3Mg⁺², 2Mg⁺² + Ni⁺², Mg⁺² + 2Ni⁺² and 3Ni⁺² species located in the mineral octahedral layer [46]. The hydroxyl stretch division is related to the M-OH bond strength change. Increasing Mg cation substitution of the original mineral structure decreases band division [46].

Spectra shown in Figs. 1b and 2(l) stand for the second and the first frequency of the OH bounded to Mg and Ni, respectively, according to the substitutions degree. The OH stretching for a talc presenting 100% of Mg cations substituted for Ni predicts the first frequency at 3627 cm^{-1} and the second at 7080 cm^{-1} attributed to OH of Ni₃OH molecule. For a talc presenting 75% of Mg cations substituted for Ni, the frequencies at 3647 cm^{-1} and 7122 cm^{-1} are attributed to OH of MgNi₂OH molecule. For a talc with 25% of Mg cations substituted for Ni the frequencies at

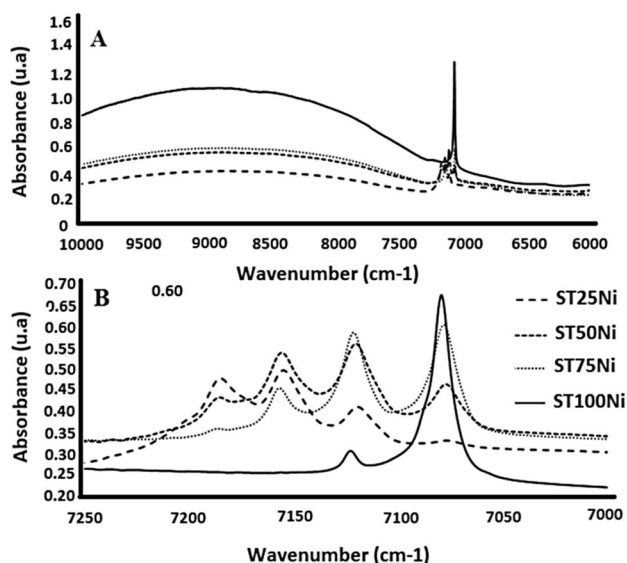


Fig. 1 Infrared spectra for $\text{Si}_4(\text{Mg}_x\text{Ni}_{1-x})_3\text{O}_{10}(\text{OH})_2$ synthetic talc **a** in the range from 10,000 to 6000 cm^{-1} ; **b** range from 7250 to 7000 cm^{-1}

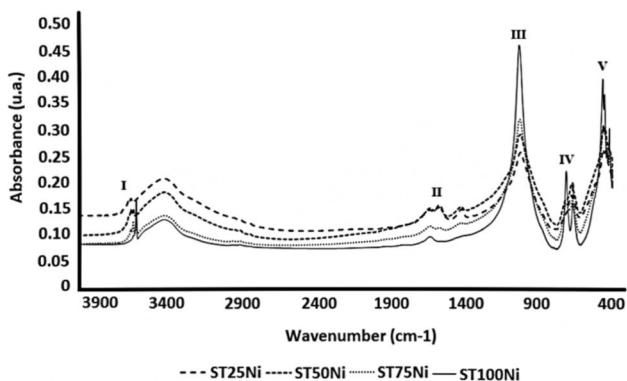


Fig. 2 Infrared spectra for $\text{Si}_4(\text{Mg}_x\text{Ni}_{1-x})_3\text{O}_{10}(\text{OH})_2$ synthetic talc

3661 cm^{-1} and 7154 cm^{-1} are related to OH of Mg_2NiOH molecule [46, 48, 49].

The frequencies at 3676 cm^{-1} and 7185 cm^{-1} are equivalent to a mineral structure presenting in its composition the molecule Mg_3OH [46, 48–50]. These bands were identified in the spectra of synthetic talcs ST25Ni and ST50Ni presenting a lower Ni percentage when compared to ST75Ni and ST100Ni. As we can see from Fig. 2(II), frequencies in the region of 1700 cm^{-1} to 1300 cm^{-1} are present in all synthetic talcs spectrum related to characteristic OH band deformation due to the presence of water [51]. In Fig. 2(III), one can observe an overlap of Si–O and Si–O–Si bands around 1025 cm^{-1} for ST25Ni, ST50Ni and ST75Ni and at 1030 cm^{-1} for ST100Ni [42, 50–52]. Frequencies in the region at 800–600 cm^{-1} are characteristic of free OH

in the synthetic talcs structure. As seen in Fig. 2(IV), the frequencies at 710–666 cm^{-1} are present for the four samples of synthetic talc [42, 50]. The bands in the region of 470–420 cm^{-1} presented in Fig. 2(V) represent the Si–O–Si overlap and the translation of the OH groups with the oxygen atoms of the octahedral sheet [42, 50, 51].

Nanocomposites infrared spectra (Fig. 3) present polyurethane characteristic bands: at 2936 cm^{-1} C–H stretching band of urethane CH_3 and CH_2 groups; at 1532 cm^{-1} attributed to H–N group and at 1245 cm^{-1} attributed to the N–C stretch [38, 39, 41]. Yet, it is possible to see a band at 1630 cm^{-1} for all nanocomposites attributed to H–O–H band of intercalated water in the talc leaves [53] or it may also be related to the Si–O vibrations of the SiO_4 molecule present in talc structure [50]. The vibration band at 1020 cm^{-1} undergoes changes in intensity while increasing synthetic talc content in nanocomposites being attributed to Si–O and Si–O–Si from synthetic and natural talc [42, 50–52]. The appearance of the band at 1630 cm^{-1} and the difference in band intensity at 1020 cm^{-1} corroborate nanocomposite formation.

3.2 DRX and TEM analysis

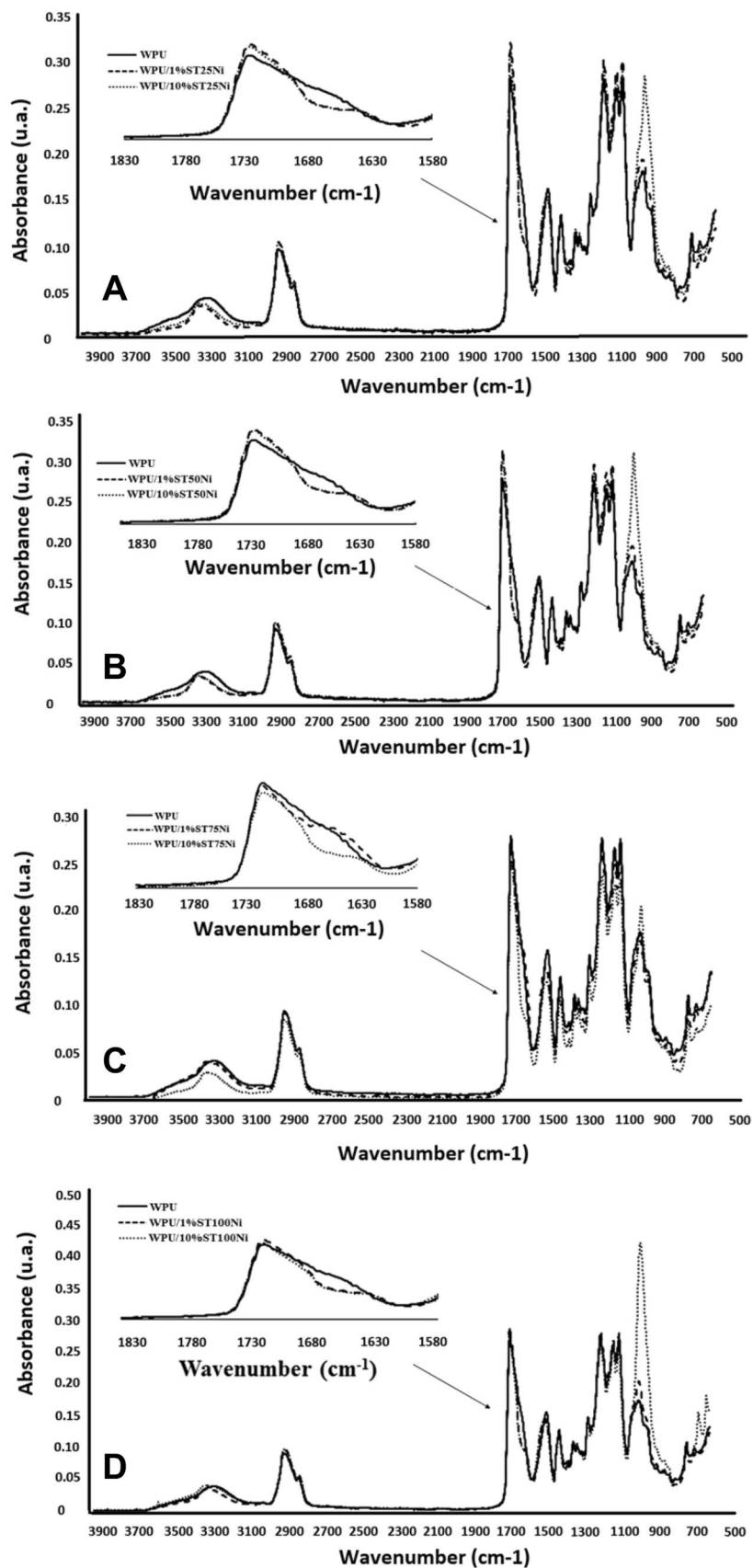
Figure 4 shows the values of the inter-reticular distance (d) of peaks 001 (9.5 Å), 002 (4.6 Å), 003 (3.1 Å), 004 (2.54 Å) and 060 (1.5 Å) characteristic of $\text{Si}_4(\text{Mg}_x\text{Ni}_{1-x})_3\text{O}_{10}(\text{OH})_2$ synthetic talc samples [35]. As the Ni amount increases in synthetic talc samples, the peaks become more intense indicating an increase in synthetic talc crystallinity [54].

Figure 5 presents XRD spectra of the WPU/STMg_xNi_y nanocomposites.

From WPU nanocomposites (1% and 10% of synthetic talc) diffractograms one can observe an intensity decrease for peaks at $2\theta = 10^\circ$ – 28° , associated to PU amorphous phase of flexible segment of WPU chain when compared to pristine WPU [55]. For nanocomposites with 10% of filler this behavior is more accentuated. The same behavior was observed by Lei et al. [27] for WPU/AEAPTMS samples indicating a good interaction filler/polymeric matrix. The appearance of peaks at $2\theta = 28^\circ$ and $2\theta = 41^\circ$ with the addition of 1% of synthetic talc referring to pristine talcs planes 003 and 004 is also observed [22, 23, 35]. With the addition of 10% of synthetic talc, peaks at $2\theta = 9^\circ$ and $2\theta = 61^\circ$ also appear, which are characteristic of pristine talc planes 001 and 060 [35, 36].

WPU nanocomposites TEM micrographs are shown in Fig. 6. Nanocomposites obtained with talc containing lower Ni content (ST25Ni and ST50Ni) present the filler predominantly in an exfoliated/intercalated form [35]. The sample with 75% of Ni (ST75Ni) presents the filler in an intercalated manner while the sample with 100% of Ni (ST100Ni) is mainly non-intercalated as already observed

Fig. 3 Infrared spectra of **a** WPU 1%ST25Ni and WPU10%ST25Ni, **b** WPU1%ST50Ni and WPU10%ST50Ni, **c** WPU 1%ST75Ni and WPU10%ST75Ni and **d** WPU 1%ST100Ni and WPU10%ST100Ni



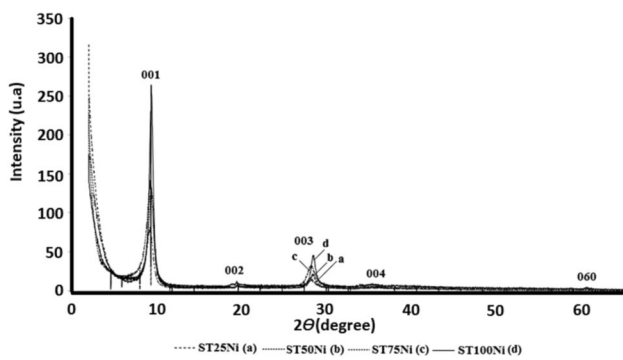


Fig. 4 X-ray diffraction patterns for $\text{Si}_4(\text{Mg}_x\text{Ni}_{1-x})_3\text{O}_{10}(\text{OH})_2$ synthetic talc

in a previously work [39]. Nanocomposite obtained with talc with 100% of Ni content (ST100Ni) shows an organization into the polymeric matrix (see Fig. 6d). As we will see

in mechanical properties section, this filler/matrix interaction/organization will positively interfere in mechanical properties.

3.3 Thermal analysis

TGA results can be observed in Table 2. Samples presented two degradation stages: The first stage is related to hard segment degradation and the second one to soft segment degradation. WPU nanocomposites prepared with the addition of 1% of synthetic talc presented similar degradation temperatures when compared to pristine WPU. With addition of 10% of ST25Ni and ST50Ni synthetic talc, the degradation temperatures slightly increase when compared to pristine WPU. Nanocomposites obtained with ST75Ni and ST100Ni showed similar degradation values to pristine WPU. This behavior may be associated with Ni amount in synthetic talc composition as observed

Fig. 5 X-ray diffraction patterns for WPU/ $\text{Si}_4(\text{Mg}_x\text{Ni}_{1-x})_3\text{O}_{10}(\text{OH})_2$ nanocomposites **A** WPU/1%/ $\text{Si}_4(\text{Mg}_x\text{Ni}_{1-x})_3\text{O}_{10}(\text{OH})_2$ [a—WPU pristine; b—WPU/1%ST25Ni; c—WPU/1%ST50Ni; d—WPU/1%ST75Ni; e—WPU/1%ST100Ni]. **B** WPU/10%/ $\text{Si}_4(\text{Mg}_x\text{Ni}_{1-x})_3\text{O}_{10}(\text{OH})_2$ [a—WPU pristine; b—WPU/10%ST25Ni; c—WPU/10%ST50Ni; d—WPU/10%ST75Ni; e—WPU/10%ST100Ni]

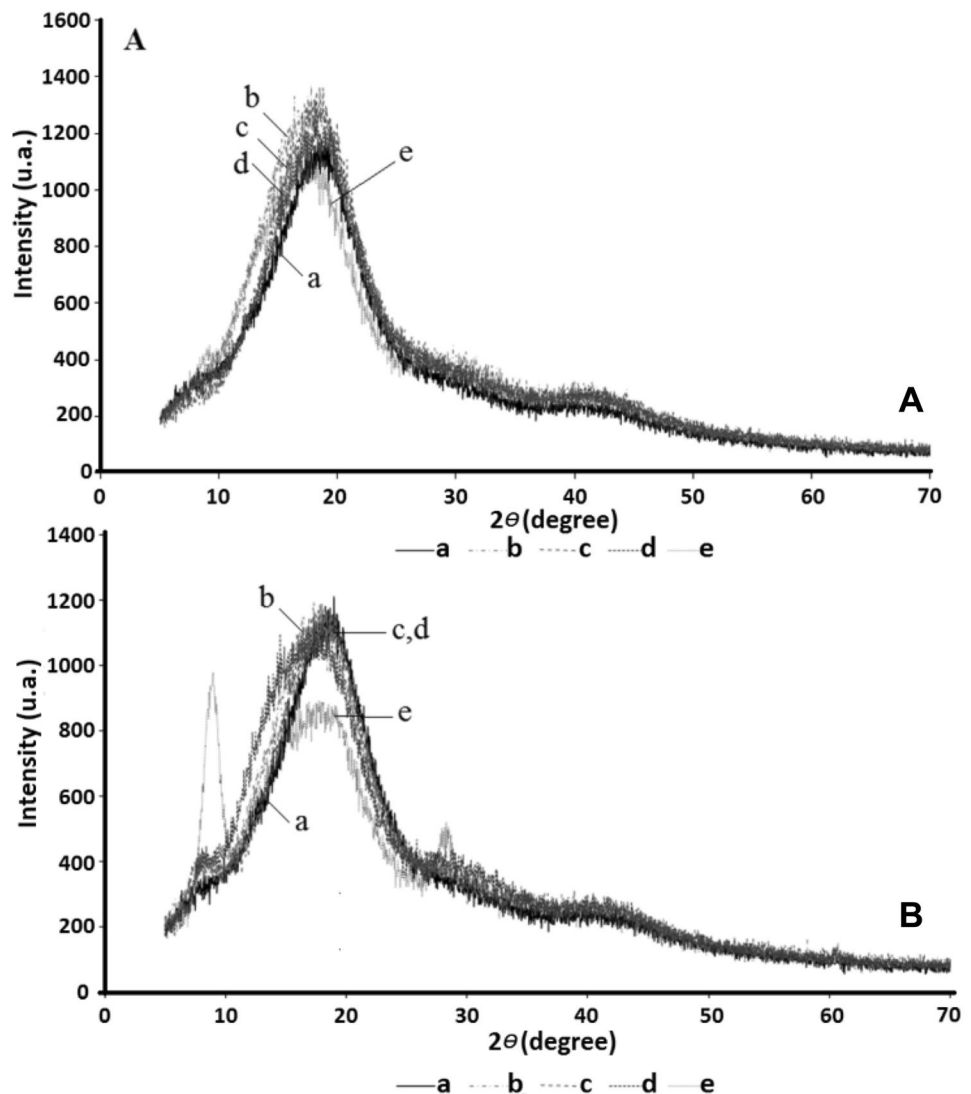


Fig. 6 TEM of WPU/ $\text{Si}_4(\text{Mg}_x\text{Ni}_{1-x})_3\text{O}_{10}(\text{OH})_2$ 10% nanocomposites samples. **a** WPU/ST25Ni; **b** WPU/ST50Ni; **c** WPU/ST75Ni; **d** WPU/ST100Ni

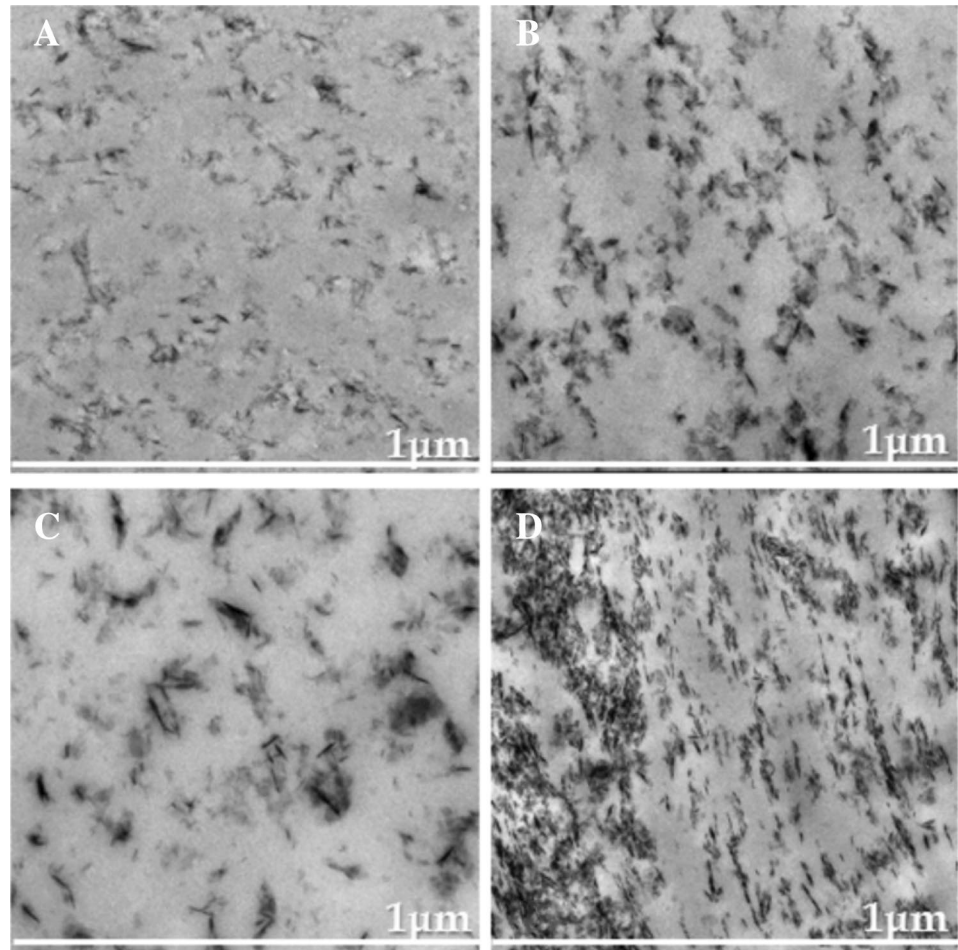


Table 2 TGA results for WPU and its nanocomposites

Sample	T_{onset} (°C)	$T_{\text{máx 1}}$ (°C)	$T_{\text{máx 2}}$ (°C)
WPU	305	342	383
WPU/ST25Ni 1%	297	335	389
WPU/ST50Ni 1%	303	344	385
WPU/ST75Ni 1%	304	340	387
WPU/ST100Ni 1%	301	345	380
WPU/ST25Ni 10%	316	373	439
WPU/ST50Ni 10%	326	380	466
WPU/ST75Ni 10%	301	340	390
WPU/ST100Ni 10%	305	346	465

for nanocomposites obtained with synthetic PU/synthetic talc-Ni100%. Literature reported that the addition of 5 wt.% of ST100Ni decreases the nanocomposites thermal stability due to charge–charge interaction [39]. The particles in a composite must be well distributed to increase film thermal resistance [56].

3.4 Mechanical analysis

Mechanical properties are presented in Figs. 7 and 8 and Table 3. It is possible to observe that for talc content of 10% an increase in Young's Modulus values was observed, [Fig. 7B; Table 3] (20.5 MPa for pristine WPU and 46.7 MPa for WPU/ST100Ni). This behavior can be associated with filler/matrix cohesive energy occurring due to the strong interaction by hydrogen bonds [41, 57] and also due to the filler organization inside polymeric matrix.

WPU nanocomposites with 1% of synthetic talc [Fig. 7A, Table 3] showed Young modulus values similar to the pristine polymeric matrix. Nanocomposites WPU/ST50Ni and WPU/ST75Ni with 1% and 10% of synthetic talc presented Young modulus values inferior when compared to pristine matrix. This may be associated with filler/filler interaction for these nanocomposites. Similar behavior was observed by Mohammadi et al. [58], in functionalized PU/ Fe_2O_3 nanocomposites.

Nanocomposites sample strain value was slightly higher when compared to pristine matrix indicating a good dispersion of the synthetic talc into the WPU matrix [39, 59].

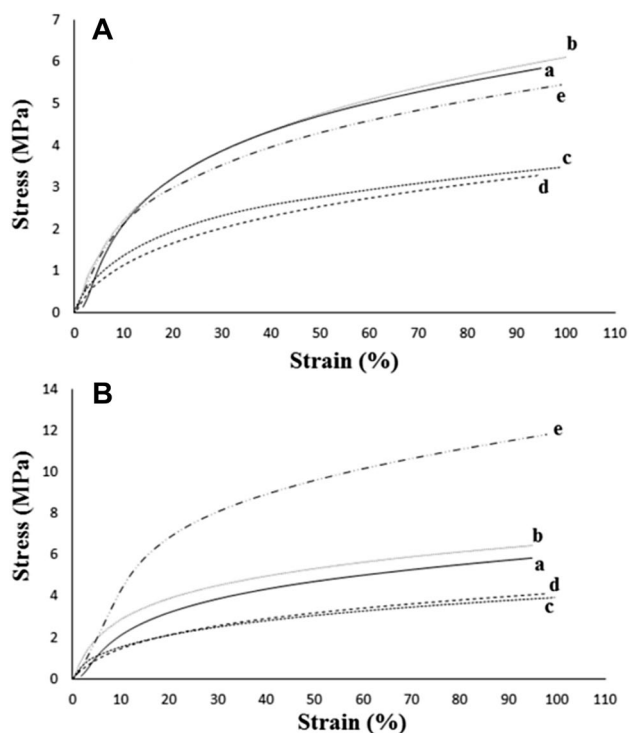


Fig. 7 DMA WPU/Si₄(Mg_xNi_{1-x})₃O₁₀(OH)₂ nanocomposites. **A** WPU/1% Si₄(Mg_xNi_{1-x})₃O₁₀(OH)₂ [a—WPU pristine; b—WPU/1%ST25Ni; c—WPU/1%ST50Ni; d—WPU/1%ST75Ni; e—WPU/1%ST100Ni]. **B** WPU/10% Si₄(Mg_xNi_{1-x})₃O₁₀(OH)₂ [a—WPU pristine; b—WPU/10%ST25Ni; c—WPU/10%ST50Ni; d—WPU/10%ST75Ni; e—WPU/10%ST100Ni]

The influence of filler good dispersion, organization into the polymeric matrix and chemical composition is also evidenced by the stress values of the nanocomposites prepared with synthetic talc with different Ni content and 10% of synthetic talc addition. Comparing samples with 50% and 100% of Ni in their chemical structure (stress value of sample WPU/ST50Ni 10% of 4.4 ± 0.4 MPa with sample WPU/ST100Ni 10% of 11.6 ± 1.0 MPa) shows that synthetic talc chemical structure can have an important influence in WPU nanocomposite mechanical properties. It is well known that nanocomposites obtained with high synthetic talc content can present important synthetic talc/synthetic talc interaction resulting in a brittle sample [56, 60]. Dos Santos [23] described that nanocomposites obtained with high amounts of synthetic talc (40%) can produce nanocomposite films with high mechanical properties [23]. These results may be associated with the nanocomposite preparation method. Physical mixture method results in nanocomposites with more efficient synthetic talc/polymer interaction when compared to the in situ method [22, 23]. The in situ method could facilitate the filler/matrix crosslink due to the chemical reaction [38, 39]. The results of the storage (E') and loss (E'') modules as well

as $\tan \delta$ for pristine WPU and nanocomposites are shown in Fig. 8.

Storage modulus (E') [Fig. 8A, B] values increase significantly with filler content increasing. The Ni content in synthetic talc composition also increases E' indicating that the presence of Ni improves the interaction of synthetic talc/WPU matrix [61, 62]. Comparing the WPU/ST25Ni nanocomposites (1% = 171 MPa and 10% = 912 MPa) and the WPU/ST100Ni nanocomposites (1% = 2086 MPa and 10% = 1814 MPa) with pristine WPU (128 MPa) it is observed the influence of filler Ni content in storage modulus values. In loss modulus analysis (Fig. 8C, D), it was noticed the presence of two peaks for pristine WPU (7 MPa and 10 MPa), related to flexible and rigid segments of polymeric matrix, respectively [63]. With synthetic talc addition (1%) the second peak shift as for ST25Ni (3 MPa and 12 MPa) and ST50Ni (7 MPa and 69 MPa). For ST75Ni (203 MPa) and ST100Ni (161 MPa), the energy of the first peak increases significantly and the second peak tends to disappear. The disappearance of the second peak shows that the interaction of synthetic talc with higher Ni content in the composition is more effective. This interaction takes place in the rigid region of the WPU matrix. With the synthetic talc addition of 10%, the second peak disappeared for all nanocomposites.

Loss modulus curves (Fig. 8C, D) show a transition peak. This peak is usually assigned to the soft segments of WPU matrix. This change in loss modulus and T_g values (WPU = 237 MPa at -24 °C; WPU/ST100Ni 1% = 158 MPa at -19 °C and WPU/ST100Ni 10% = 102 MPa at -18 °C) could be related to the good incorporation and distribution of the fillers into WPU chains [64]. Higher values for storage modulus, loss modulus and T_g peak indicated strong adhesion of the fillers into the WPU matrix, as previously reported by our group [22].

3.5 Morphological analysis

Figure 9 presents the FESEM micrographs for pristine WPU and for the nanocomposites with addition of 1% and 10% of Si₄(Mg_xNi_{1-x})₃O₁₀(OH)₂ synthetic talcs.

All samples present cracks. WPU nanocomposites images show rough surfaces similar to pristine WPU matrix. FESEM images indicate a homogeneous filler distribution for all nanocomposites showing that the WPU may be interacting with the filler [27]. Filler good distribution into the polymeric matrix is one of the factors interfering in nanocomposite mechanical properties, as observed by Peng [65] for WPU nanocomposites with a natural fibrillary mineral clay.

Figure 10 shows AFM images for all samples of nanocomposites and pristine WPU.

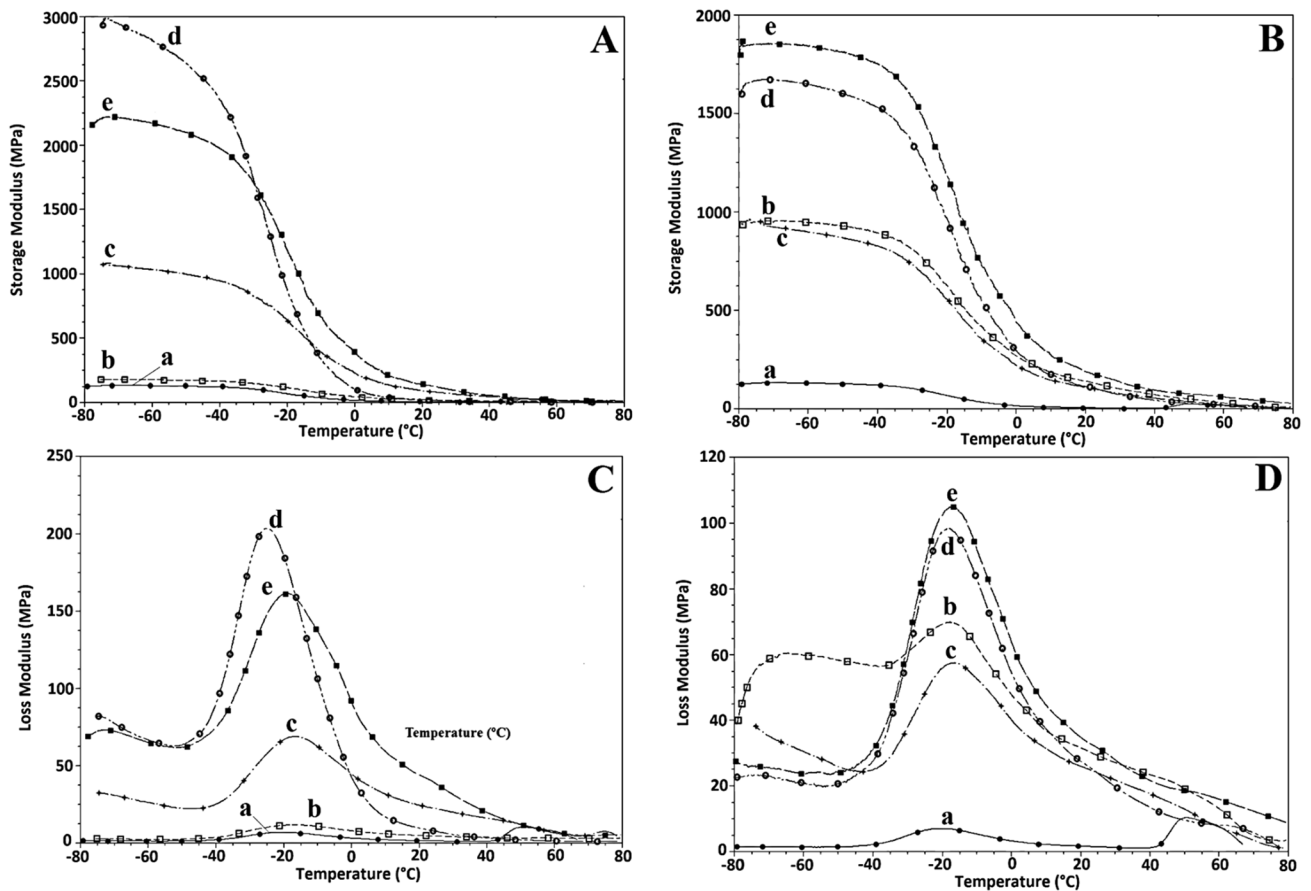


Fig. 8 A Storage modulus WPU/1% $\text{Si}_4(\text{Mg}_x\text{Ni}_{1-x})_3\text{O}_{10}(\text{OH})_2$ and **C** loss modulus WPU/1% $\text{Si}_4(\text{Mg}_x\text{Ni}_{1-x})_3\text{O}_{10}(\text{OH})_2$; [a—WPU pristine; b—WPU/1%ST25Ni; c—WPU/1%ST50Ni; d—WPU/1%ST75Ni].

B Storage modulus WPU/10% $\text{Si}_4(\text{Mg}_x\text{Ni}_{1-x})_3\text{O}_{10}(\text{OH})_2$ and **D** loss modulus WPU/10% $\text{Si}_4(\text{Mg}_x\text{Ni}_{1-x})_3\text{O}_{10}(\text{OH})_2$. [a—WPU pristine; b—WPU/10%ST25Ni; c—WPU/10%ST50Ni; d—WPU/10%ST75Ni]

Table 3 DMA results for WPU and its nanocomposites

Sample	Stress (MPa)	Strain (%)	Young modulus (MPa)
WPU	5.9 ± 0.7	94.5 ± 0.7	20.5 ± 1.6
WPU/ST25Ni 1%	5.8 ± 0.4	97.8 ± 1.7	22.5 ± 1.6
WPU/ST50Ni 1%	3.7 ± 0.5	97.8 ± 1.2	14.0 ± 2.0
WPU/ST75Ni 1%	3.7 ± 0.6	94.9 ± 0.4	11.3 ± 2.7
WPU/ST100Ni 1%	5.4 ± 0.1	99.8 ± 0.1	20.9 ± 1.2
WPU/ST25Ni 10%	6.4 ± 0.6	96.7 ± 1.5	30.1 ± 2.2
WPU/ST50Ni 10%	4.4 ± 0.4	99.6 ± 0.2	16.6 ± 0.3
WPU/ST75Ni 10%	4.4 ± 0.4	97.6 ± 0.5	16.4 ± 3.2
WPU/ST100Ni 10%	11.6 ± 1.0	97.7 ± 0.5	46.7 ± 3.9

WPU matrix presents dark and bright areas corresponding to amorphous (flexible segments) and crystalline domains (rigid segments), respectively [66]. With synthetic talc addition rearrangements can take place into

the polymeric matrix structure depending on the synthetic talc/WPU interaction. For higher filler content, the interaction synthetic talc/polymer matrix becomes more intense changing the polymer matrix organization as seen in Fig. 10. Increasing Ni content in the synthetic talc chemical structure a tendency of a small separation among hard and soft segments is also observed and could be related with polymer chain reorganization due to the interaction of synthetic talc/polymer matrix taking place in the rigid region of the WPU matrix as observed in the Loss modulus test. Yet, the synthetic talc/synthetic talc interaction can occur with higher filler contents [23]. In samples with 10% of synthetic talc it is possible to visualize more intense bright spots on the matrix surface attributed to agglomerated particles in synthetic talc/synthetic talc form [25].

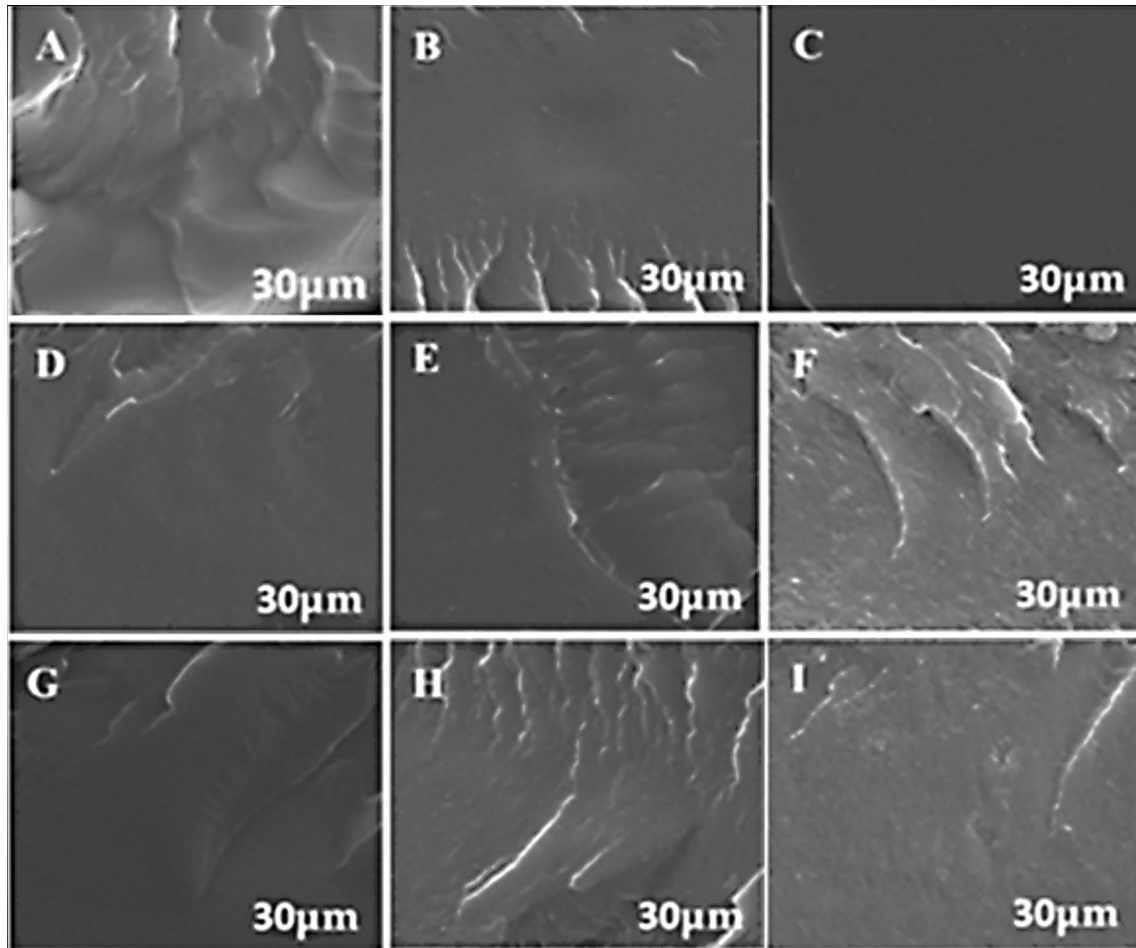


Fig. 9 FESEM of film surface **a** WPU pristine. **b** From to **e** samples WPU/ $\text{Si}_4(\text{Mg}_x\text{Ni}_{1-x})_3\text{O}_{10}(\text{OH})_2$ 1% nanocomposites—**b** WPU/ST25Ni, **c** WPU/ST50Ni, **d** WPU/ST75Ni and **e** WPU/ST100Ni. **f** From to **i** WPU/ $\text{Si}_4(\text{Mg}_x\text{Ni}_{1-x})_3\text{O}_{10}(\text{OH})_2$ 10% nanocomposites—**f** WPU/ST25Ni, **g** WPU/ST50Ni, **h** WPU/ST75Ni and **i** WPU/ST100Ni

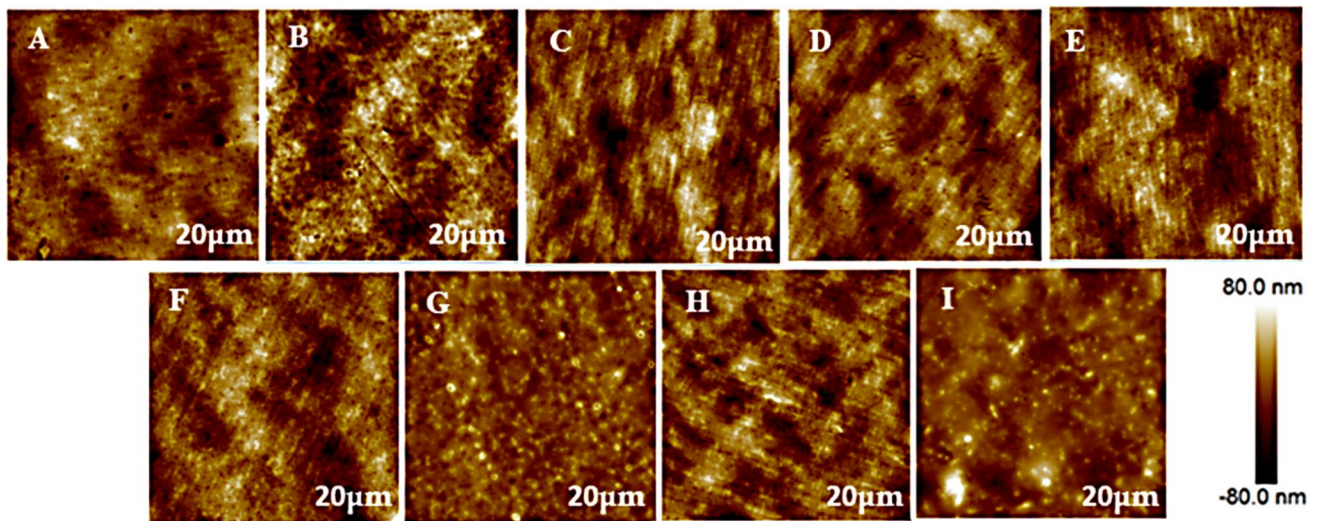


Fig. 10 AFM images. **a** WPU pristine. **b** to **e** samples WPU/1% $\text{Si}_4(\text{Mg}_x\text{Ni}_{1-x})_3\text{O}_{10}(\text{OH})_2$ nanocomposites—**b** WPU/ST25Ni, **c** WPU/ST50Ni, **d** WPU/ST75Ni and **e** WPU/ST100Ni. **f** to **i** WPU/10% $\text{Si}_4(\text{Mg}_x\text{Ni}_{1-x})_3\text{O}_{10}(\text{OH})_2$ nanocomposites—**f** WPU/ST25Ni, **g** WPU/ST50Ni, **h** WPU/ST75Ni and **i** WPU/ST100Ni

4 Conclusions

WPU/Si₄(Mg_xNi_{1-x})₃O₁₀(OH)₂ nanocomposites were prepared by physical mixing. Synthetic talc presents different chemical composition in relation to Mg and Ni content occurring in the octahedral sheets of synthetic talc structure. FTIR, DRX and TEM analyses demonstrate the good synthetic talc/WPU matrix interaction. FESEM and AFM showed a homogeneous distribution of talc particles for all samples. Improvements in nanocomposites mechanical properties in relation to the pristine WPU matrix were observed for samples with higher synthetic talc content. The variation of the amount of Mg and Ni in synthetic talc composition altered the storage and loss module results being higher for nanocomposites obtained with synthetic talc with higher Ni content in their compositions. The Tg varied according to synthetic talc content. Synthetic talc with different metal content in their composition may alter thermal and mechanical properties of WPU nanocomposites and can thus be designed for several applications.

Acknowledgments GD and MP thank CAPES for their PhD scholarship. SE acknowledges CNPq for PQ Grant. This study was financed in part by the Coordenação de Aperfeiçoamento de Pessoal de Nível Superior—Brasil (CAPES)—Finance Code 001. Thanks to Nokxeller—Microdispersions by the supply of part of the reagents used in this work.

Compliance with ethical standards

Conflict of interest The authors declare that there is no conflict of interest.

References

- Bae SY, Jeong SH, Kim BK (2016) Waterborne polyurethane elastomer using renewable polyols. *J Elastomers Plast* 48(1):47–57
- Zhou X, Fang C, Lei W, Su J, Li L, Li Y (2017) Thermal and crystalline properties of waterborne polyurethane by in situ water reaction process and the potential application as biomaterial. *Prog Org Coat* 104:1–10
- Zhou X et al (2015) Recent advances in synthesis of waterborne polyurethane and their application in water-based ink: a review. *J Mater Sci Technol* 31(7):708–722
- Sultan M, Islam A, Gull N, Bhatti HN, Safa Y (2015) Structural variation in soft segment of waterborne polyurethane acrylate nanoemulsions. *J Appl Polym Sci* 132(12):1–10
- Liu N et al (2015) The effects of the molecular weight and structure of polycarbonatediols on the properties of waterborne polyurethanes. *Prog Org Coat* 82:46–56
- García-Pacios V, Jofre-Reche JA, Costa V, Colera M, Martín-Martínez JM (2013) Coatings prepared from waterborne polyurethane dispersions obtained with polycarbonates of 1,6-hexanediol of different molecular weights. *Prog Org Coat* 76(10):1484–1493
- El-Sayed AA, Salama M, Salem T, Rehan M (2016) Synergistic combination of reduction and polymerization reactions to prepare silver/waterborne polyurethane nanocomposite for coating applications. *Indian J Sci Technol* 9(17):1–10
- Mumtaz F, Zuber M, Zia KM, Jamil T, Hussain R (2013) Synthesis and properties of aqueous polyurethane dispersions: influence of molecular weight of polyethylene glycol. *Korean J Chem Eng* 30(12):2259–2263
- Gurunathan T, Rao CRK, Narayan R, Raju KVS (2013) Synthesis, characterization and corrosion evaluation on new cationomeric polyurethane water dispersions and their polyaniline composites. *Prog Org Coat* 76(4):639–647
- Mao H, Wang C, Wang Y (2015) Synthesis of polymeric dyes based on waterborne polyurethane for improved color stability. *New J Chem* 39(5):3543–3550
- Heck CA, dos Santos JHZ, Wolf CR (2015) Waterborne polyurethane: the effect of the addition or in situ formation of silica on mechanical properties and adhesion. *Int J Adhes Adhes* 58:13–20
- Sardon H, Irusta L, Aguirresarobe RH, Fernández-Berridi MJ (2014) Polymer/silica nanohybrids by means of tetraethoxysilane sol–gel condensation onto waterborne polyurethane particles. *Prog Org Coat* 77(9):1436–1442
- Chen C, Wu W, Xu WZ, Charpentier PA (2017) The effect of silica thickness on nano TiO₂ particles for functional polyurethane nanocomposites. *Nanotechnology* 28(11):115709
- Hormaiztegui MEV, Mucci VL, Santamaria-Echart A, Corcuera MÁ, Eceiza A, Aranguren MI (2016) Waterborne polyurethane nanocomposites based on vegetable oil and microbrillated cellulose. *J Appl Polym Sci* 133(47):1–12
- Nisar M, Bergmann C, Geshev J, Quijada R, Galland GB (2016) An efficient approach to the preparation of polyethylene magnetic nanocomposites. *Polymer* 97:131–137
- Chen S, Chen S, Zhao G, Chen J (2015) Fabrication and properties of novel superparamagnetic, well—dispersed waterborne polyurethane/Ni–Zn ferrite nanocomposites. *Compos Sci Technol* 119:108–114
- Sardon H, Irusta L, Fernández-Berridi MJ, Lansalot M, Bourgeat-Lami E (2010) Synthesis of room temperature self-curable waterborne hybrid polyurethanes functionalized with (3-aminopropyl)triethoxysilane (APTES). *Polymer* 51(22):5051–5057
- Ding X et al (2020) Preparation of waterborne polyurethane-silica nanocomposites by a click chemistry method. *Mater Today Commun* 23:100911
- Li L, Xu L, Ding W, Lu H, Zhang C, Liu T (2019) Molecular-engineered hybrid carbon nanofillers for thermoplastic polyurethane nanocomposites with high mechanical strength and toughness. *Compos B Eng* 177:107381
- Sanusi OM, Benelfellah A, Ait Hocine N (2020) Clays and carbon nanotubes as hybrid nanofillers in thermoplastic-based nanocomposites—a review. *Appl Clay Sci* 185:105408
- Chen S, Jin T, Wu W, Zhao G (2016) Novel environmentally friendly waterborne polyurethane/hollow Ni_{0.3}Zn_{0.5}Fe₂O₄ nanocomposite films: superior magnetic and mechanical properties. *RSC Adv* 6(79):75440–75448
- Dias G et al (2018) Analyzing the influence of different synthetic talcs in waterborne polyurethane nanocomposites obtainment. *J Appl Polym Sci* 135(14):1–8
- Dos Santos LM et al (2017) Waterborne polyurethane/Fe₃O₄-synthetic talc composites: synthesis, characterization, and magnetic properties. *Polym Bull* 75(5):1915–1930
- Shahrousvand M, Hoseinian MS, Ghollasi M, Karbalaieimahi A, Salimi A, Tabar FA (2017) Flexible magnetic polyurethane/Fe₂O₃ nanoparticles as organic-inorganic nanocomposites for biomedical applications: properties and cell behavior. *Mater Sci Eng C* 74:556–567

25. Zhang S, Li Y, Peng L, Li Q, Chen S, Hou K (2013) Synthesis and characterization of novel waterborne polyurethane nanocomposites with magnetic and electrical properties. *Compos A Appl Sci Manuf* 55:94–101
26. Chiorcea-Paquim A-M, Diculescu VC, Cervini P, Cavalheiro ETG, Oliveira Brett AM (2014) Graphite–castor oil polyurethane composite electrode surfaces—AFM morphological and electrochemical characterisation. *J Electroanal Chem* 731:172–178
27. Lei L, Xia Z, Zhang L, Zhang Y, Zhong L (2016) Preparation and properties of amino-functional reduced graphene oxide/waterborne polyurethane hybrid emulsions. *Prog Org Coat* 97:19–27
28. Kannan M, Thomas S, Joseph K (2017) Flame-retardant properties of nanoclay-filled thermoplastic polyurethane/polypropylene nanocomposites. *J Vinyl Add Technol* 23(2):E72–E80
29. Piszczek Ł, Danowska M, Mielarek-Kropidłowska A, Szyszka M, Strankowski M (2014) Synthesis and thermal studies of flexible polyurethane nanocomposite foams obtained using nanoclay modified with flame retardant compound. *J Therm Anal Calorim* 118(2):901–909
30. Stratigaki M, Choudalakis G, Gotsis AD (2014) Gas transport properties in waterborne polymer nanocomposite coatings containing organomodified clays. *J Coat Technol Res* 11(6):899–911
31. Dumas A, Martin F, Ferrage E, Micoud P, Le Roux C, Petit S (2013) Synthetic talc advances: coming closer to nature, added value, and industrial requirements. *Appl Clay Sci* 85:8–18
32. Dumas A et al (2013) Phyllosilicates synthesis: a way of accessing edges contributions in NMR and FTIR spectroscopies. Example of synthetic talc. *Phys Chem Miner* 40(4):361–373
33. Ashenai Ghasemi F, Ghasemi I, Menbari S, Ayaz M, Ashori A (2016) Optimization of mechanical properties of polypropylene/talc/graphene composites using response surface methodology. *Polym Test* 53:283–292
34. Espinosa KR, Castillo LA, Barbosa SE (2016) Blown nanocomposite films from polypropylene and talc. Influence of talc nanoparticles on biaxial properties. *Mater Des* 111:25–35
35. Dumas A, Mizrahi M, Martin F, Requejo FG (2015) Local and extended-order evolution of synthetic talc during hydrothermal synthesis: extended X-ray absorption fine structure, X-ray diffraction, and Fourier transform infrared spectroscopy studies. *Cryst Growth Des* 15(11):5451–5463
36. Dumas A et al (2016) Fast-geomimicking using chemistry in supercritical water. *Angew Chem Int Ed* 55(34):9868–9871
37. Claverie M et al (2018) Synthetic talc and talc-like structures: preparation, features and applications. *Chem Eur J* 24(3):519–542
38. Dias G et al (2016) Comparing different synthetic talc as fillers for polyurethane nanocomposites. *Macromol Symp* 367(1):136–142
39. Prado MA et al (2015) Synthetic Ni-talc as filler for producing polyurethane nanocomposites. *J Appl Polym Sci* 132(16):1–8
40. Dias G et al (2018) Synthetic talc as a new platform for producing fluorescent clay polyurethane nanocomposites. *Appl Clay Sci* 158:37–45
41. dos Santos LM et al (2015) New magnetic nanocomposites: polyurethane/Fe₃O₄-synthetic talc. *Eur Polym J* 69:38–49
42. Martin F et al (1999) The structural formula of talc from the trimouns deposit, Pyrenees, France. *Can Mineral* 37:997–1006
43. Lebre C (2007) Elaboration et caractérisation de talcs synthétiques pour l'amélioration des propriétés physiques des matériaux composites industriels
44. Martin F et al (2019) A review of Ni and Co incorporation during talc synthesis: applications to crystal chemistry, industrial compounds and natural Ni- and Co-rich ore. *J Geochem Explor* 200:27–36
45. Dias G et al (2020) Synthetic talc as catalyst and filler for waterborne polyurethane-based nanocomposite synthesis. *Polym Bull* 77(2):975–987
46. Wilkins RWT, Ito J (1967) Infrared spectra of some synthetic talcs. *Am Mineral* 52:1649–1661
47. Ferrage E, Martin F, Micoud P, Petit S, Guesde J (2003) Cation site distribution in clinoclones: a NIR approach. *Clay Miner* 38:329–338
48. Petit S, Decarreau A, Martin F, Buchet R (2004) Refined relationship between the position of the fundamental OH stretching and the first overtones for clays. *Phys Chem Miner* 31(9):585–592
49. Blanchard M et al (2018) Infrared spectroscopic study of the synthetic Mg–Ni talc series. *Phys Chem Miner* 45(9):843–854
50. Zhang M (2006) Dehydroxylation, proton migration, and structural changes in heated talc: an infrared spectroscopic study. *Am Mineral* 91(5–6):816–825
51. Chabrol K et al (2010) Functionalization of synthetic talc-like phyllosilicates by alkoxyorganosilane grafting. *J Mater Chem* 20(43):9695–9706
52. Ulian G, Tosoni S, Valdrè G (2013) Comparison between Gaussian-type orbitals and plane wave ab initio density functional theory modeling of layer silicates: talc [Mg₃Si₄O₁₀(OH)₂] as model system. *J Chem Phys* 139(20):204101
53. Farmer VC (1958) The infra-red spectra of talc, saponite, and hectorite. *Mineral Mag J Mineral Soc* 31(241):829–845
54. Reinholdt M, Brendlé J, Tuilier M-H, Kaliaguine S, Ambroise E (2013) Hydrothermal synthesis and characterization of Ni-Al montmorillonite-like phyllosilicates. *Nanomaterials* 3(1):48–69
55. Lee HT, Lin LH (2006) Waterborne polyurethane/clay nanocomposites: novel effects of the clay and its interlayer ions on the morphology and physical and electrical properties. *Macromolecules* 39(18):6133–6141
56. Kim YJ, Kim BK (2014) Synthesis and properties of silanized waterborne polyurethane/graphene nanocomposites. *Colloid Polym Sci* 292(1):51–58
57. Pokharel P, Choi S, Lee DS (2015) The effect of hard segment length on the thermal and mechanical properties of polyurethane/graphene oxide nanocomposites. *Compos Part A Appl Sci Manuf* 69:168–177
58. Mohammadi A, Barikani M, Lakouraj MM (2016) Biocompatible polyurethane/thiacalix[4]arenes functionalized Fe₃O₄ magnetic nanocomposites: synthesis and properties. *Mater Sci Eng C* 66:106–118
59. Dias G et al (2015) Synthetic silico-metallic mineral particles (SSMMP) as nanofillers: comparing the effect of different hydrothermal treatments on the PU/SSMMP nanocomposites properties. *Polym Bull* 72(11):2991–3006
60. Pokharel P, Lee DS (2014) High performance polyurethane nanocomposite films prepared from a masterbatch of graphene oxide in polyether polyol. *Chem Eng J* 253:356–365
61. Mishra AK, Mishra RS, Narayan R, Raju KVS (2010) Effect of nano ZnO on the phase mixing of polyurethane hybrid dispersions. *Prog Organ Coat* 67(4):405–413
62. Wang X et al (2016) Enhanced mechanical and barrier properties of polyurethane nanocomposite films with randomly distributed molybdenum disulfide nanosheets. *Compos Sci Technol* 127:142–148
63. Kim BK, Seo JW, Jeong HM (2003) Morphology and properties of waterborne polyurethane/clay nanocomposites. *Eur Polym J* 39(1):85–91
64. Cao X, Habibi Y, Lucia LA (2009) One-pot polymerization, surface grafting, and processing of waterborne polyurethane-cellulose nanocrystal nanocomposites. *J Mater Chem* 19:7137–7145

65. Peng L, Zhou L, Li Y, Pan F, Zhang S (2011) Synthesis and properties of waterborne polyurethane/attapulgite nanocomposites. *Compos Sci Technol* 71(10):1280–1285
66. Santamaria-Echart A, Ugarte L, García-Astrain C, Arbelaiz A, Corcuera MA, Eceiza A (2016) Cellulose nanocrystals reinforced environmentally-friendly waterborne polyurethane nanocomposites. *Carbohydr Polym* 151:1203–1209

Publisher's Note Springer Nature remains neutral with regard to jurisdictional claims in published maps and institutional affiliations.